Optical Materials xxx (2016) 1–9

Contents lists available at ScienceDirect

Optical Materials

journal homepage: www.elsevier.com/locate/optmat

Europium(III)-doped $A_2Hf_2O_7$ (A = Y, Gd, Lu) nanoparticles: Influence of annealing temperature, europium(III) concentration and host cation on the luminescent properties

Jelena Papan [a], Dragana J. Jovanović [a], Katarina Vuković [a], Krisjanis Smits [b], Vesna Đorđević [a], Miroslav Dramićanin [a, *]

[a] Vinča Institute of Nuclear Sciences, University of Belgrade, P.O. Box 522, 11001, Serbia
[b] Institute of Solid State Physics, University of Latvia, 8 Kengaraga Street, Riga, LV-1063, Latvia

ARTICLE INFO

Article history:
Received 15 December 2015
Accepted 6 April 2016
Available online xxx

Keywords:
Rare earth hafnate
Phosphor
Luminescence
Judd-Ofelt
Europium(III)

ABSTRACT

The detailed analyses of structure and luminescence of europium(III)-doped $A_2Hf_2O_7$ (A = Y, Gd, Lu) nanoparticles is presented. Samples were prepared by time and cost effective combustion method that utilize polyethylene glycol both as a chelating agent and as a fuel, with different europium(III) concentrations (from 1 to 12 at.%), annealed at temperatures ranging from 800 to 1400 °C, and with alternating A^{3+} cation in the $A_2Hf_2O_7$ host. Then, structural variations between materials were analysed by X-ray diffraction and structural refinement, while the changes in the luminescence were assessed from the Judd-Ofelt analyses of emission spectra. Nanoparticles prepared at the lowest temperature (800 °C) had the smallest particle size of ~6 nm and showed the highest quantum efficiency when doped with 1 and 2 at.% of europium(III). Radiative transition rate and quantum efficiency of emission showed $Lu_2Hf_2O_7 > Gd_2Hf_2O_7 > Y_2Hf_2O_7$ trend.

1. Introduction

Compounds of general formula $A_2B_2O_7$, where A element is a rare earth (RE) or an element with inert lone-pair of electrons and B element is a transition metal with variable oxidation state or a post transition metal, display interesting physical properties like high melting point (~2700 K), catalytic activity, piezoelectric behaviour, ferro- and ferrimagnetism, giant magnetoresistance, and could be used as solid oxide fuel cells, dielectric materials, catalysts, immobilizers of nuclear waste and hosts for luminescent materials [1–5]. To achieve electroneutrality in these compounds, two combinations of A and B cations are possible A^{3+}/B^{4+} or A^{2+}/B^{5+}. Crystal structures of $A_2B_2O_7$ are in direct correlation with the ratio of their ionic radii, rA^{3+}/rB^{4+}. If the ratio is low ($rA^{3+}/rB^{4+} < 1.46$) they crystallize in fluorite crystal structure with $Fm\bar{3}$ m symmetry, where both cations are in 8-fold coordination with one anion vacancy per unit cell. In the case where $r(A^{3+})$ is larger and/or $r(B^{4+})$ is smaller, the ratio is larger ($rA^{3+}/rB^{4+} = 1.46–1.78$), and these materials crystallize in pyrochlore crystal structure with $Fd\bar{3}$ m symmetry, where A^{3+} is also in the 8-fold coordination while B^{4+} is in 6-fold coordination [6,7].

In the field of transition metal or lanthanide doped materials for luminescence applications, $A_2B_2O_7$ compounds activated with Mn^{4+} have been used as deep-red emitting phosphors for white LEDs [8,9], and as conventional downconversion phosphors when activated with Eu^{3+} and Sm^{3+} [10,11]. Also, these materials could be applied as scintillators due to their high density (7.93–9.95 g cm^{-3}) [12] which results in the excellent gamma-ray stopping power, and in the computer tomography and positron emission tomography [13]. Recently, luminescence thermometry with Eu^{3+} and Sm^{3+} doped $Gd_2Ti_2O_7$ has been demonstrated [14,15]. To date, only few reports have been published on the synthesis of rare earth based $A_2B_2O_7$ (A = Y, Gd, Lu; B = Ti^{4+}, Hf^{4+}, Sn^{4+}, Zr^{4+}) pyrochlores and on their luminescence when doped with trivalent rare earths, even though they are promising candidates for the activation with trivalent rare earth ions due to similarities of ionic radii and valence [16]. $Y_2Hf_2O_7$ was synthetized with a classic solid-state method, while $Gd_2Hf_2O_7$ by a vaporization method [17,18]. However, the disadvantage of these synthesis methods is the use of high temperatures (1300–1900 °C) or high pressures [18,19]. The use of soft

* Corresponding author.
E-mail address: dramican@vinca.rs (M. Dramićanin).

http://dx.doi.org/10.1016/j.optmat.2016.04.007
0925-3467/

chemical synthesis methods, Pechini modification of self-propagating high-temperature synthesis, co-precipitation, and combustion synthesis has yielded a cost-effective preparation of $Y_2Hf_2O_7$ [13,20,21]. Until now, properties of $Y_2Hf_2O_7$ phosphors doped with La^{3+} and Ti^{4+} ions, and $Lu_2Hf_2O_7$ doped with Tb^{3+} ions have been reported [22–24].

In this work we show time and cost effective synthesis of high-density $A_2Hf_2O_7$ nanoparticles by combustion method that utilize polyethylene glycol (PEG) both as a chelating agent and as a fuel. Then, we systematically analyse how structure of nanoparticles and emission of europium(III) ions that are introduced into nanoparticles depends on the variation of nanoparticle's composition and on the temperature of synthesis. For this purpose nanoparticles are prepared at 800, 1100 and 1400 °C, europium(III) concentration is varied between 1 and 12 at.%, and, finally, different A^{3+} cations (Y, Gd, Lu) were used for the $A_2Hf_2O_7$ host. Judd-Ofelt theory was applied for the analysis of europium(III) emission which allowed calculation and comparison of radiative and nonradiative transition rates, Judd-Ofelt intensity parameters, and quantum efficiencies.

2. Experimental

All chemicals: $HfCl_4$ (99.9%, Alfa Aesar) Y_2O_3 (99.9%, Alfa Aesar), Eu_2O_3 (99.9%, Alfa Aesar), HNO_3 (69–70%, J.T. Baker), NH_3 (30–33%, Roth) and PEG 200 (Alfa Aesar) were of the highest purity available and were used without any further purification. The direct use of $HfCl_4$ in the synthesis is undesirable because Cl^- ions could quench optical signal [25]. To eliminate Cl^- ions, $HfCl_4$ was first dissolved in water and Hf^{4+} ions formed HfO^{2+}. These ions are then transformed in $HfO(OH)_2$ in the presence of aqueous 6.7 M ammonia solution and precipitate was washed until pH value was neutral to remove access of Cl^- and NH_4^+ ions. The obtained precipitate ($HfO(OH)_2$) was used further in the synthesis after dissolution in HNO_3 acid as shown in the following three steps:

$$HfCl_4 + H_2O \rightarrow HfO^{2+} + 2H^+ + 4Cl^-$$

$$HfO^{2+} + 2NH_4OH \rightarrow HfO(OH)_2\downarrow + 2NH_4^+$$

$$HfO(OH)_2 + 4HNO_3 \rightarrow Hf(NO_3)_4 + 3H_2O$$

In the obtained $Hf(NO_3)_4$ transparent solution an appropriate amounts of Y_2O_3 and corresponding stoichiometric ratio Eu_2O_3 (x = 1, 2, 4, 8, 12 at.%) were added, and the mixture was stirred at 80 °C. After 1 h solution becomes transparent and PEG 200 was added to the solution in the 1:1 ratio (to the mass of $Y_2Hf_2O_7$). Solution was further heated at 120 °C until it formed the gel, which was then transferred to the crucible and calcined at different temperatures (T = 800, 1100 i 1400 °C) for 24 h. The europium(III) −doped $Gd_2Hf_2O_7$ and $Lu_2Hf_2O_7$ samples were obtained under identical experimental procedure and conditions.

XRD measurements were obtained using a Rigaku Smart Lab diffractometer. Diffraction data were recorded in a 2θ range from 10° to 90°, counting 0.7°/min in 0.02° steps. The structural analysis results (unit cell parameter, crystal coherence size, microstrain values, and data fit parameters) were obtained using PDXL Integrated X-ray powder diffraction software.

Luminescence measurements were obtained at room temperature with Fluorolog-3 Model FL3-221 spectrofluorometer system (Horiba JobinYvon), utilizing a 450 W Xenon lamp as an excitation source for steady-state emission measurements, and a Xenon−Mercury pulsed lamp for emission decay measurements.

Transmission electron microscopy (TEM) studies were made on a Tecnai G20 (FEI) operated at an accelerating voltage of 200 kV. Samples were supported on a perforated carbon film (S147-4, Agar scientific) and were dried in air for one day. It was observed that at a high electron radiation dose defects were induced into the crystals until their crystal structure disappeared. Therefore, for HRTEM images the electron beam intensity was reduced strongly by inserting a condenser aperture and by decreasing the spot size.

3. Results and discussion

3.1. Structure and morphology of nanoparticles

Typical HRTEM images of $Y_2Hf_2O_7$ nanoparticles doped with 2 at.% of europium(III) and annealed at different temperatures are shown in Fig. 1a, b, c. All samples reveals clear crystal structure visible in HRTEM images and also in SADP. The SADP and reconstructed electron diffraction pattern of sample annealed in 800 °C is shown Fig. 1a (right side) and corresponds to cubic structure. The crystallite sizes for sample annealed at 800 °C was in range from 3 till 7 nm, whereas for sample annealed at 1100 °C in range from 5 till 15 nm. The crystallite size distribution and average size 11.7 nm of sample annealed in 1100 °C was estimated from TEM DF images and are shown in Fig. 1b (right side) together with selected DF images. The particles of sample annealed at 1400 °C was too large to evaluate the crystallite size in TEM. All samples shows nanoparticle agglomerates with different sizes (Fig. 1c (right side)), and particle size up to 300 nm for sample annealed at 1400 °C.

Fig. 2a displays XRD patterns of the $Y_2Hf_2O_7$:2 at.% Eu^{3+} samples annealed at different temperatures (T = 800, 1100 and 1400 °C) for 24 h, while Table 1 presents structural parameters of the samples obtained after Rietveld refinement of experimental data. All patterns clearly show presence of the cubic fluorite structure ($Fm\bar{3}$ m (2 2 5)) in samples, with diffraction peaks indexed according to the ICDD 00-024-1406 card. With the increase of annealing temperature diffraction peaks became narrower and an average crystallite size of powders increases from 6 nm to 66 nm. The calculated average crystalline sizes for samples annealed at 800 °C and 1100 °C are very close to that observed in TEM images. The increase in annealing temperature did not significantly alter the unit cell parameter (*a*), therefore, the local environments around dopant europium(III) ions are similar in all samples in term of the distance between europium(III) and neighbouring ions. However, the values of microstrain are ten times lower in samples annealed at higher temperatures. XRD patterns of the $A_2Hf_2O_7$:1 at.% Eu^{3+} (A = Y, Gd, Lu) samples and structural parameters of the samples obtained after Rietveld refinement of experimental data are presented in Fig. S1. The patterns clearly show pure cubic fluorite structure (*Fmm* (2 2 5)) in the samples, with diffraction peaks indexed according to the ICDD 00-024-1406 card (for A = Y and Lu) and ICDD 00-024-0425 (for A = Gd).

Fluorite $Y_2Hf_2O_7$ crystallize in space group $Fm\bar{3}$ $m(O_h^5)$ No.225, with one formula unit in the primitive cell; the basic crystallographic properties are listed in Table 2. Y^{3+} and Hf^{4+} cations randomly occupy $m\bar{3}$ *m* site, each having occupancy factor of 0.5. To maintain charge balance, there are seven oxygens and a vacancy occupying $\bar{4}$ 3 *m* site of the unit cell, as can be seen in Fig. 2b. In this type of oxygen deficient fluorite structure the occupancy for each anion site is 0.875, where any of the eight oxygen sites in the structure have an equal probability to become vacant. In Fig. 2b blue spheres represent cations, red spheres represent oxygen's, while yellow sphere is the vacancy. Blue tetrahedrons are coordination polyhedra around oxygens, yellow tetrahedron is the vacancy coordination polyhedron that also retains the shape in the crystalline structure, while coordination polyhedrons around cations are cubes as presented in red on the picture. In the 8-fold coordination, the values of ionic radii of constituting cations are:

Please cite this article in press as: J. Papan, et al., Europium(III)-doped $A_2Hf_2O_7$ (A = Y, Gd, Lu) nanoparticles: Influence of annealing temperature, europium(III) concentration and host cation on the luminescent properties, Optical Materials (2016), http://dx.doi.org/10.1016/j.optmat.2016.04.007

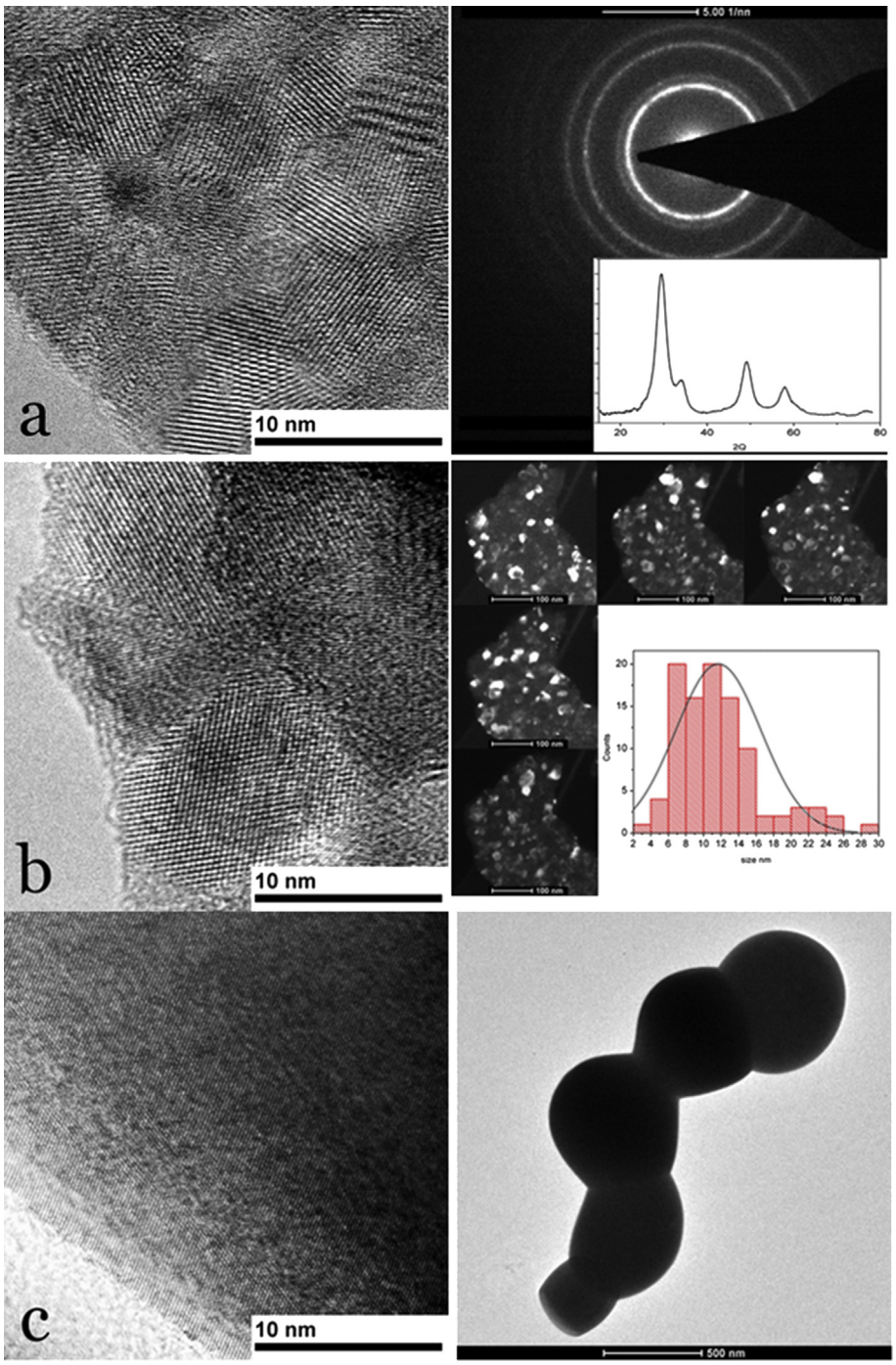

Fig. 1. TEM images for $Y_2Hf_2O_7$ nanoparticles annealed at: a) T = 800 °C (left) with selected area electron diffraction pattern (right), b) T = 1100 °C (left) with the crystaline size distribution and selected TEM DF image (right), c) T = 1400 °C – high magnification (left) and low magnification (right).

r^{3+}_{VIII} (Y) = 1.019 Å, r^{3+}_{VIII} (Gd) = 1.053 Å, r^{3+}_{VIII} (Lu) = 0.977 Å, r^{4+}_{VIII} (Hf) = 0.83 Å, which gives r(Y^{3+}/Hf^{4+}) = 1.23, r(Gd^{3+}/Hf^{4+}) = 1.27 and r(Lu^{3+}/Hf^{4+}) = 1.18 [16]. In the pyrochlore structure, hafnium(IV) ion is in 6-fold coordination and value of ionic radius is r^{4+}_{VI} (Hf) = 0.71 Å, that was taken into account for rA^{3+}/rB^{4+} in previous reports [1,2]. The ionic radius for dopant europium(III) ion is r^{3+}_{VIII} (Eu) = 1.066 Å [16], that gives great probability of isomorphic ion exchange in the fluorite $A_2Hf_2O_7$ structure, without significant disturbing of the lattice. The surrounding of europium(III) in the crystal lattice is cube, but the oxygen vacancy significantly changes the symmetry of the crystal field effecting the luminescence properties.

3.2. Luminescent properties

The representative excitation and emission luminescence spectra of europium(III)-doped $Y_2Hf_2O_7$ nanoparticles annealed at 800 °C are presented in Fig. 3. Fig. 3a shows excitation spectrum in the 350–550 nm spectral range (recorded at λ_{max} = 612 nm) that is composed of characteristic europium(III) absorption bands

Please cite this article in press as: J. Papan, et al., Europium(III)-doped $A_2Hf_2O_7$ (A = Y, Gd, Lu) nanoparticles: Influence of annealing temperature, europium(III) concentration and host cation on the luminescent properties, Optical Materials (2016), http://dx.doi.org/10.1016/j.optmat.2016.04.007

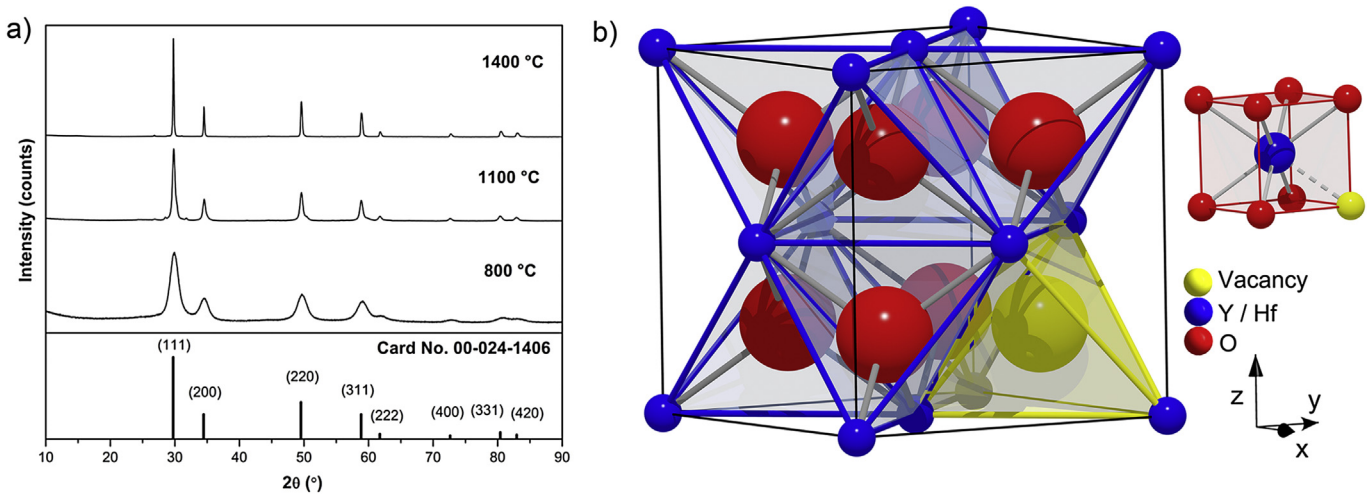

Fig. 2. a) XRD patterns of $Y_2Hf_2O_7$: 2 at.%Eu^{3+} annealed at different temperatures (T = 800, 1100 and 1400 °C) and b) the schematic representation of $Y_2Hf_2O_7$ oxygen deficient fluorite-type crystal structure with oxygen and vacancy coordination polyhedrons shown in the unit cell, and the local environment of the Y/Hf cations shown on the right.

Table 1
Structural parameters of $Y_2Hf_2O_7$: 2 at.%Eu^{3+}samples annealed at different temperatures (800, 1100 i 1400 °C) for 24 h.

Parameter	800 °C	1100 °C	1400 °C
a (Å)	5.19920 (6)	5.21227 (17)	5.19985 (17)
Crystallite size (nm)	5.83	13.32	66.60
Microstrain (%)	1.19 (21)	0.14 (5)	0.1589 (11)
Rwp (%)[a]	3.17	5.48	4.72
Re (%)[b]	1.99	1.91	1.98
GOF[c]	1.5911	2.8705	2.3830

[a] Rwp – regression sum of weighted squared errors of fit.
[b] Re -regression sum of relative errors of fit.
[c] GOF - goodness-of-fit (= Rwp/Re).

centered at 361 nm ($^7F_0 \rightarrow {}^5D_4$), 380 nm ($^7F_0 \rightarrow {}^5G_2$), 393 nm ($^7F_0 \rightarrow {}^5L_6$), 413 nm ($^7F_1 \rightarrow {}^5L_6$), 464 nm ($^7F_0 \rightarrow {}^5D_2$), and 531 nm ($^7F_1 \rightarrow {}^5D_1$) [8].

Emission spectrum, Fig. 3b, is recorded at room temperature in the 550–750 nm spectral range with excitation in the $^5D_2$ level of europium(III). Single emission peak at 579 nm originate from $^5D_0 \rightarrow {}^7F_0$ transition of europium(III) ions [26,27]. Stark components of magnetic-dipole transition $^5D_0 \rightarrow {}^7F_1$ are located around 591 nm; intensity of this transition does not depend on the local environment, therefore it can be used as a reference for Judd-Ofelt calculations [28]. The most intensive transition is centered at 612 nm; this transition corresponds to the electric-dipole $^5D_0 \rightarrow {}^7F_2$ transition and it is hypersensitive on the local environment of europium(III) ions [29]. The ratio of intensities of $^5D_0 \rightarrow {}^7F_2$ and $^5D_0 \rightarrow {}^7F_1$ is often termed as asymmetric ratio and presents the indirect measure of the disorder around europium(III) ions [30]. Two week emissions at 654 and 707 nm correspond to $^5D_0 \rightarrow {}^7F_3$ and $^5D_0 \rightarrow {}^7F_4$ transitions [31].

3.2.1. Judd-Ofelt calculations

Transition probabilities of the rare earths are composed mainly of the electric dipole contribution $^5D_0 \rightarrow {}^7F_J$ (J = 2, 4, 6) and to a much lesser extent by the magnetic-dipole contribution $^5D_0 \rightarrow {}^7F_1$. The $^5D_0 \rightarrow {}^7F_3$ transition is forbidden according to Judd-Ofelt theory, both in magnetic and induced electric dipole scheme, and this transition can only gain intensity via J-mixing [32,33]. Moreover, according to the standard Judd-Ofelt theory the $^5D_0 \rightarrow {}^7F_0$ transition is strictly forbidden. Due to the above mentioned, these two transitions will not be considered in determining of transition probabilities and Judd-Ofelt parameters. The intensity of $^5D_0 \rightarrow {}^7F_1$ magnetic dipole transition is largely independent of the environment and can be considered in a first approximation to be constant [34].

The Judd-Ofelt theory is a powerful tool for analysing 4f–4f electronic transitions in lanthanide series [35,36]. Study of the optical properties of the rare earth ions in different host materials provides information about radiative and nonradiative emission rates, branching ratio, and quantum efficiency of emission.

In the standard theory radiative transition probability, *A*, of spontaneous emission of a transition between two manifolds J and J′ is given by:

$$A\left(\Psi J;\Psi' J'\right) = \frac{64\pi^4 e^2}{3h(2J+1)\lambda^3}\left[n\left(\frac{n^2+2}{9}\right)^2 D_{ED} + n^2 D_{MD}\right], \qquad (1)$$

where *h* denotes Planck constant (6.63×10^{-27} erg s), $2J + 1$ is the degeneracy of the initial state, *n* is the refractive index and *e* is charge of electron. The electric and magnetic dipole strengths, respectively, D_{ED} and D_{MD} are given by Ref. [37].

$$D_{MD} = 9.6 \times 10^{-42}\ \text{esu}^2\text{cm}^2 \qquad (2)$$

Table 2
Basic crystallographic properties of the fluorite $A_2Hf_2O_7$ ($Fm\bar{3}\,m$) structure.

No	Atom	Oxidation	Multiplicity	Wyckoff	Site symmetry	Coordinates			Site occupancy
						x	y	z	
1	A	+3	2	4a	$m\bar{3}m$	0	0	0	0.5
2	Hf	+4	2	4a	$m\bar{3}m$	0	0	0	0.5
3	O	−2	7	8c	$\bar{4}3m$	0.25	0.25	0.25	0.875

Please cite this article in press as: J. Papan, et al., Europium(III)-doped $A_2Hf_2O_7$ (A = Y, Gd, Lu) nanoparticles: Influence of annealing temperature, europium(III) concentration and host cation on the luminescent properties, Optical Materials (2016), http://dx.doi.org/10.1016/j.optmat.2016.04.007

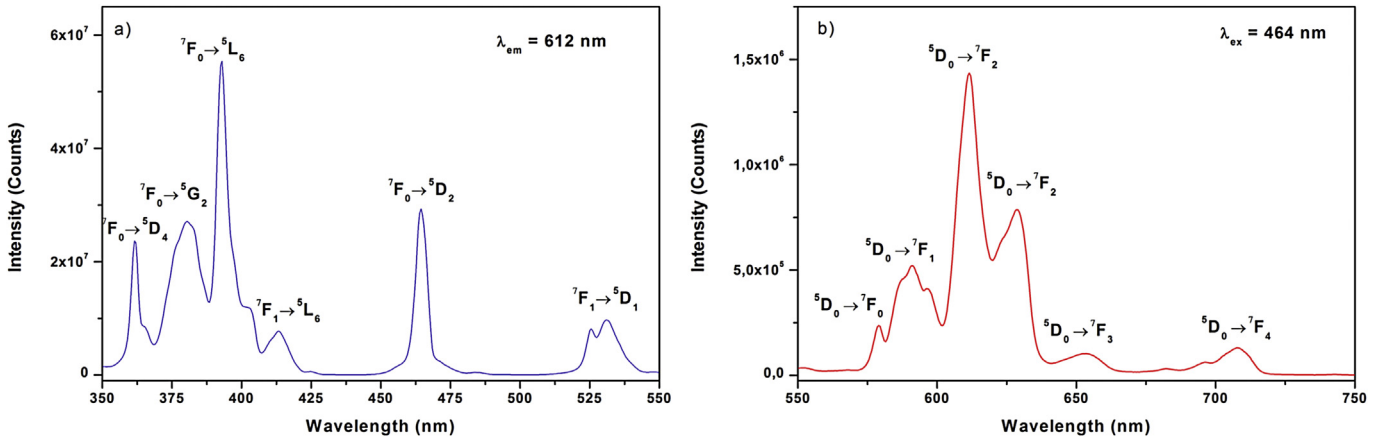

Fig. 3. a) Excitation spectrum (λ_{em} = 612 nm) and b) emission spectrum ((λ_{ex} = 464 nm) of $Y_2Hf_2O_7$:2 at.% Eu^{3+} nanoparticles measured at room temperature.

and the strength of all induced electric dipole transitions is:

$$D_{ED}(\Psi J, \Psi' J') = e^2 \sum_{\lambda=2,4,6} \Omega_\lambda |\langle \Psi J \| U^{(\lambda)} \| \Psi J' \rangle|^2, \quad (3)$$

where squared reduced matrix elements $\left|\langle \Psi J \| U^{(\lambda)} \| \Psi J' \rangle\right|^2$ have values independent of the host matrix. For calculation of intensity parameters, Ω_λ ($\lambda = 2, 4$ and 6), the following equation can be used [27,38]:

$$\Omega_\lambda = \frac{D_{MD}\nu_1^3}{e^2\nu_\lambda^3} \frac{9n^3}{n(n^2+2)^2 |\langle \Psi J \| U^{(\lambda)} \| \Psi' J' \rangle|^2} \frac{\int I_\lambda(\nu_\lambda)}{\int I_1(\nu_1)}, \quad (4)$$

where non-diagonal elements of the $\left|\langle \Psi J \| U^{(\lambda)} \| \Psi J' \rangle\right|^2$ matrix have zero values, and values of squared reduced matrix element for the $^5D_0 \rightarrow {}^7F_2$ transition is 0.0032 and 0.0023 for the $^5D_0 \rightarrow {}^7F_4$ transition [39].

For calculation, the value of refractive index of 1.691 is taken from the literature [40].

We have calculated radiative emission probabilities of all transitions originating from the $^5D_0$ excited state in terms of the ratio of areas S under corresponding emission curves [27,38]:

$$A(^5D_0 \rightarrow {}^7F_{2,4}) = A(^5D_0 \rightarrow {}^7F_1) \times \frac{S(^5D_0 \rightarrow {}^7F_{2,4})}{S(^5D_0 \rightarrow {}^7F_1)}. \quad (5)$$

The total radiative emission rate, A_R, for an excited state is given as the sum of all radiative rates:

$$A_R = \sum_{\lambda=1,2,4} A_\lambda. \quad (6)$$

The radiative lifetime (τ_R) of an excited level $\Psi' J'$ is given by the reciprocal of the total radiative transition rates (A_R). Using calculated lifetime values and total radiative transition rates one can calculate non-radiative transition rate A_{NR} (which includes relaxation by multiphonon emission and effective energy transfer rates arising from ion-ion interactions):

$$A_{NR} = \frac{1}{\tau_R} - A_R. \quad (7)$$

Then, the quantum efficiency of emission η is:

$$\eta = \frac{A}{A_R + A_{NR}}. \quad (8)$$

This quantity represents he ratio between the number of photons emitted by the europium(III) ion to the number of those absorbed.

The asymmetry ratio R can be considered as indicative of the asymmetry of the coordination environment around the europium(III) ion. Higher values of R indicate higher asymmetry around the trivalent europium ions [41,42]. Ω_2 and R affirm similar physical information on the bonding nature between europium(III) and the surrounding anions. Ω_2 parameter depends on the local environment around the europium(III) site and it is affected by the covalence between europium(III) and ligand anions, whereas Ω_4 and Ω_6 are related to the viscosity and rigidity of the host material in which the ions are situated. Ω_6 intensity parameter could not be determined because $^5D_0 \rightarrow {}^7F_6$ emission in this sample couldn't be detected due to the instrumental limitations.

3.2.2. *Influence of annealing temperature on europium(III) emission*

Judd-Ofelt calculations were used to analyse emission spectra of $Y_2Hf_2O_7$ nanoparticles doped with 2 at.% of europium(III) that were prepared at 800, 1100, 1400 °C. Table 3 comprises values of Judd-Ofelt intensity parameters, experimental lifetime, radiative and non-radiative transition rates, quantum efficiencies and asymmetry ratios; their temperature dependences are depicted in Fig. 4.

For all annealing temperatures europium(III) emission was characterized with $\Omega_2 > \Omega_4$, Fig. 4a. According Kumar et al. [42] this trend confirms the covalence between europium(III) ions and ligands, as well as the asymmetry around europium(III) site. One can notice that Ω_2, Ω_4 and R (Fig. 4b) decrease with the annealing temperature increase. Both R and Ω_2 reveal information on the short range structural ordering around europium(III); the higher the values of R and Ω_2 the lower the symmetry around the europium(III) [43,44]. This result can be correlated with results of structural analyses (Table 1) which showed significant (an order of magnitude) decrease of microstrain in samples annealed at high temperatures.

Sample prepared at 800 °C has the largest values of radiative transition rate and quantum efficiency. At larger temperatures, 1100 °C and 1400 °C, radiative transition rates and quantum efficiencies decrease, Fig. 4c and d. Stronger and more efficient emission could be ascribed to the disrupted symmetry around europium(III) in sample prepared at 800 °C which has much larger microstrain and smaller particle size compared to the samples

Please cite this article in press as: J. Papan, et al., Europium(III)-doped $A_2Hf_2O_7$ (A = Y, Gd, Lu) nanoparticles: Influence of annealing temperature, europium(III) concentration and host cation on the luminescent properties, Optical Materials (2016), http://dx.doi.org/10.1016/j.optmat.2016.04.007

Table 3
Judd-Ofelt intensity parameters, experimental lifetimes, radiative and non-radiative transition rates, quantum efficiencies and asymmetry ratios of europium(III) emission from $Y_2Hf_2O_7$ nanoparticles prepared at 800, 1100 and 1400 °C.

T (°C)	Ω_2 (10^{-20} cm^{-2})	Ω_4 (10^{-20} cm^{-2})	τ (ms)	A_R (s^{-1})	A_{NR} (s^{-1})	η (%)	R
800	6.88	3.65	1.54	444.61	204.73	68.47	4.25
1100	5.40	2.34	1.72	371.75	209.63	63.94	3.32
1400	3.84	1.64	1.67	285.06	313.47	47.60	2.37

synthesized at higher temperatures. We should mention that the values of quantum efficiency are slightly underestimated, since calculation does not account $^5D_0 \rightarrow {}^7F_{3,5,6}$ emissions. However, the trend of quantum efficiency change with annealing temperature is unaffected by this calculation deficiency.

3.2.3. Concentration dependence of europium(III) emission

Concentration effect on europium(III) emission is analysed from emission spectra of $Y_2Hf_2O_7$ nanoparticles prepared at 800 °C with 1, 2, 4, 8 and 12 at.% of europium. Results of Judd-Ofelt analyses are presented in Table 4 and Fig. 5.

Judd-Ofelt intensity parameters and asymmetry ratio did not show significant variations with the change of europium(III) concentration, Fig. 5a and b. The highest quantum efficiency values of 69.5% and 68.5% are obtained for 1 and 2 at.% doping, respectively. Reduction of quantum efficiency with the concentration increase, Fig. 5d, is a result of the intensification of non-radiative transition rate, Fig. 5c, due to the stronger energy migration between the neighbouring europium(III) owing to reduced distances between ions when concentration is high [45–47].

3.2.4. Variations in europium(III) emission between hosts with different A^{3+} cation: $A_2Hf_2O_7$ (A = Y, Gd, Lu)

Small differences of Y(III), Gd(III) and Lu(III) properties, in particular the ion radius values, provide slightly different local environments for dopant europium(III) ions. Emission spectra of $Y_2Hf_2O_7$, $Gd_2Hf_2O_7$ and $Lu_2Hf_2O_7$ samples prepared at 800 °C with 1 at.% europium were analysed with Judd-Ofelt theory and the results are presented in Table 5 and Fig. 6.

The highest values of quantum efficiency (~76.5%), lifetime and Ω_2 are found for $Lu_2Hf_2O_7$ host as a consequence of the largest intensity parameters; the lowest value of ~69% is obtained for $Y_2Hf_2O_7$.

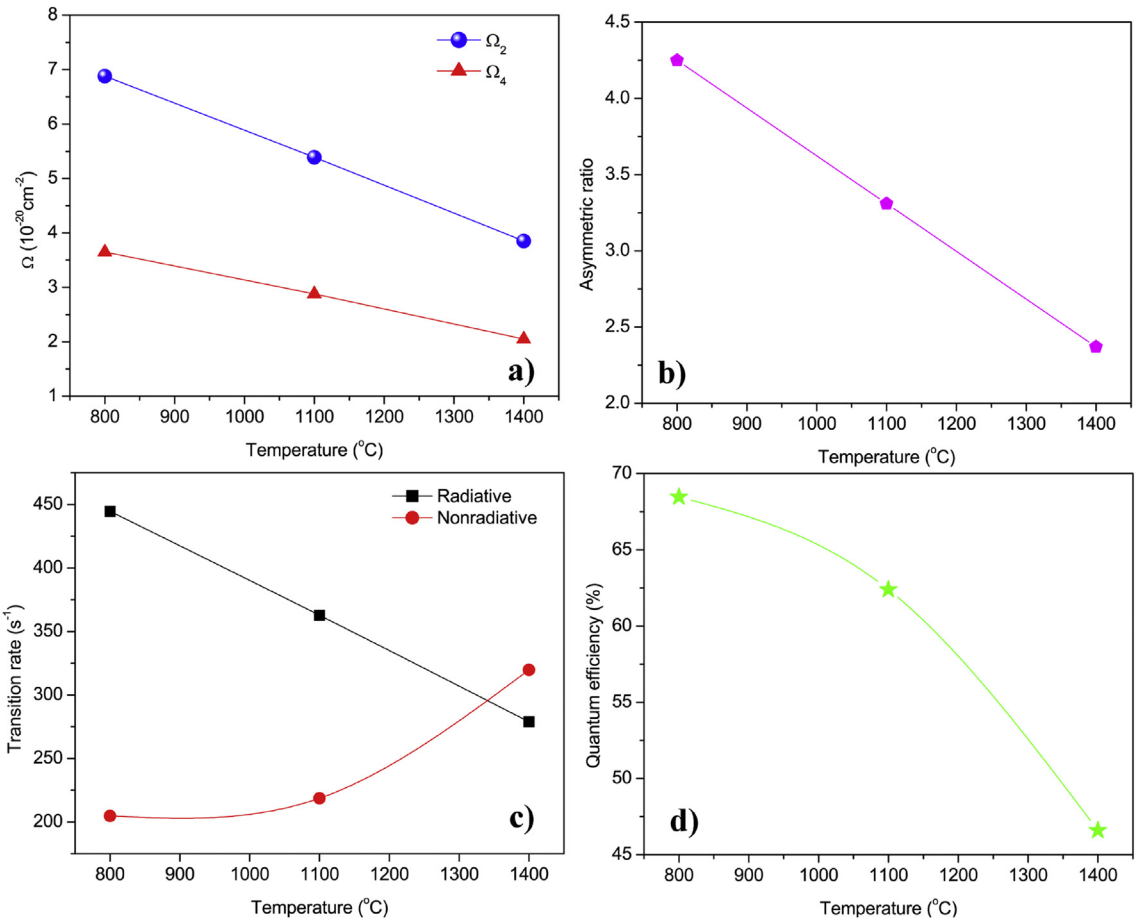

Fig. 4. a) Ω_2 (blue spheres) and Ω_4 (red triangles) Judd-Ofelt intensity parameters, b) asymmetry ratio, c) radiative (black squares) and nonradiative transition rates (red circles), and d) quantum efficiency of europium(III) emission in $Y_2Hf_2O_7$ nanoparticles prepared at 800, 1100 and 1400 °C. (For interpretation of the references to colour in this figure legend, the reader is referred to the web version of this article.)

Please cite this article in press as: J. Papan, et al., Europium(III)-doped $A_2Hf_2O_7$ (A = Y, Gd, Lu) nanoparticles: Influence of annealing temperature, europium(III) concentration and host cation on the luminescent properties, Optical Materials (2016), http://dx.doi.org/10.1016/j.optmat.2016.04.007

Table 4
Judd-Ofelt intensity parameters, experimental lifetimes, radiative and non-radiative transition rates, quantum efficiencies and asymmetry ratios of europium(III) emission from $Y_2Hf_2O_7$ nanoparticles prepared at 800 °C with 1, 2, 4, 8 and 12 at.% of europium.

Conc.(at%)	Ω_2 (10^{-20} cm^{-2})	Ω_4 (10^{-20} cm^{-2})	τ (ms)	A_R (s^{-1})	A_{NR} (s^{-1})	η (%)	R
1	7.03	3.64	1.53	454.39	199.20	69.52	4.38
2	6.88	3.65	1.54	444.61	204.73	68.47	4.25
4	7.01	3.87	1.47	458.25	226.67	66.91	4.37
8	6.78	4.06	1.45	452.65	246.64	64.73	4.23
12	6.51	4.16	1.38	442.75	281.88	61.11	4.06

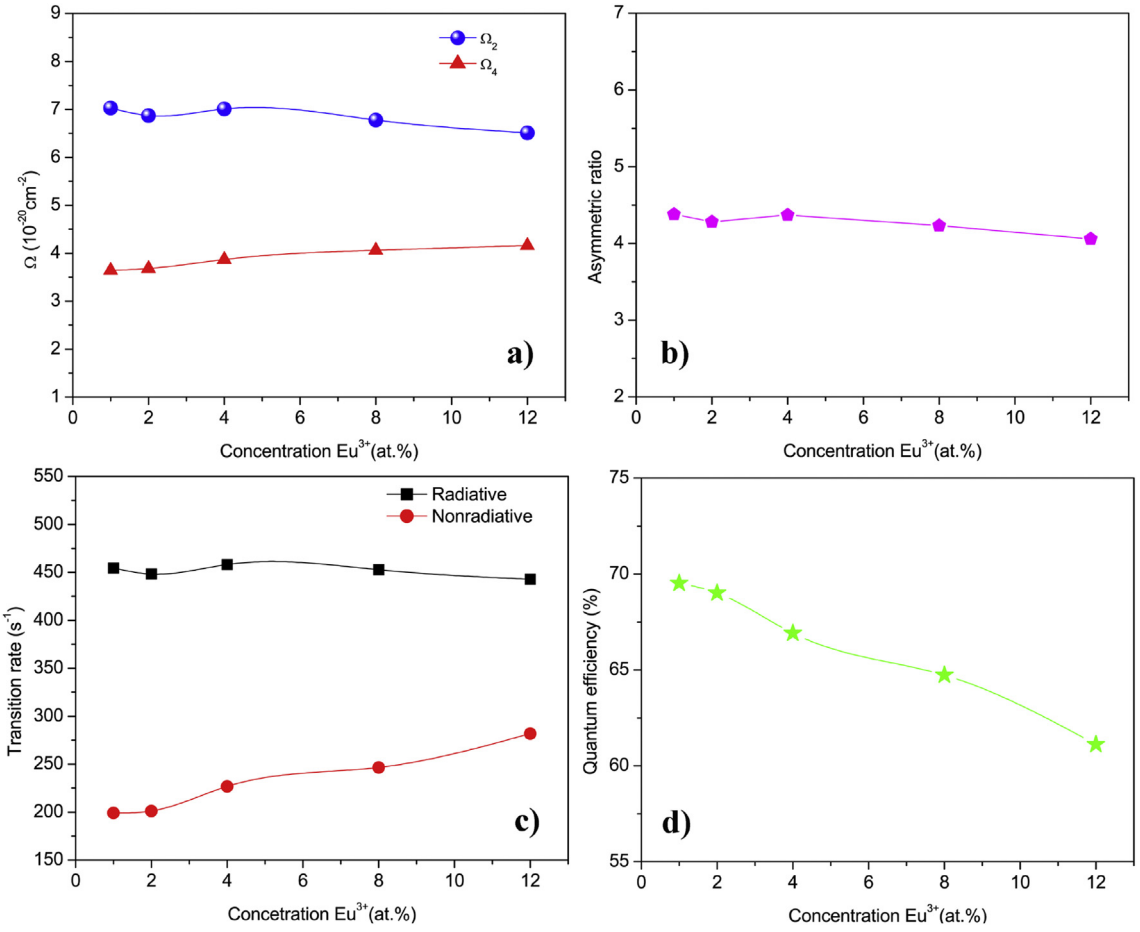

Fig. 5. a) Ω_2 (blue spheres) and Ω_4 (red triangles) Judd-Ofelt intensity parameters, b) asymmetric ratio, c) radiative (black squares) and nonradiative transition rates (red circles), and d) quantum efficiency of europium(III) emission from $Y_2Hf_2O_7$ nanoparticles prepared at 800 °C with 1, 2, 4, 8 and 12 at.% of europium. (For interpretation of the references to colour in this figure legend, the reader is referred to the web version of this article.)

Table 5
Judd-Ofelt intensity parameters, experimental lifetimes, radiative and non-radiative transition rates, quantum efficiencies and asymmetry ratios of europium(III) emission from $A_2Hf_2O_7$ (A = Y, Gd, Lu) hosts prepared at 800 °C with 1 at.% europium.

Host	Ω_2 (10^{-20} cm^{-2})	Ω_4 (10^{-20} cm^{-2})	τ (ms)	A_R (s^{-1})	A_{NR} (s^{-1})	η (%)	R
$Y_2Hf_2O_7$	7.03	3.64	1.53	454.39	199.20	69.22	4.38
$Gd_2Hf_2O_7$	7.68	3.77	1.51	480.19	182.05	72.51	4.74
$Lu_2Hf_2O_7$	7.75	3.73	1.58	483.72	149.02	76.42	4.80

4. Conclusion

To conclude, the combustion synthesis method that utilize polyethylene glycol as a chelating agent and as a fuel can be used for preparation of nanoparticles of rare earth hafnate fluorites $A_2Hf_2O_7$ (A = Y, Gd, Lu). Nanoparticles of different sizes from 6 nm to 300 nm are obtained by varying annealing temperature from 800 °C to 1400 °C. Higher annealing temperatures reduce micro-strain and enlarge crystallite size of samples but do not affect the size of unit cell. Europium(III) emission has the highest quantum efficiency in nanoparticles prepared at 800 °C with 1 to 2 at.% doping concentration. Also, quantum efficiencies of europium(III)

Please cite this article in press as: J. Papan, et al., Europium(III)-doped $A_2Hf_2O_7$ (A = Y, Gd, Lu) nanoparticles: Influence of annealing temperature, europium(III) concentration and host cation on the luminescent properties, Optical Materials (2016), http://dx.doi.org/10.1016/j.optmat.2016.04.007

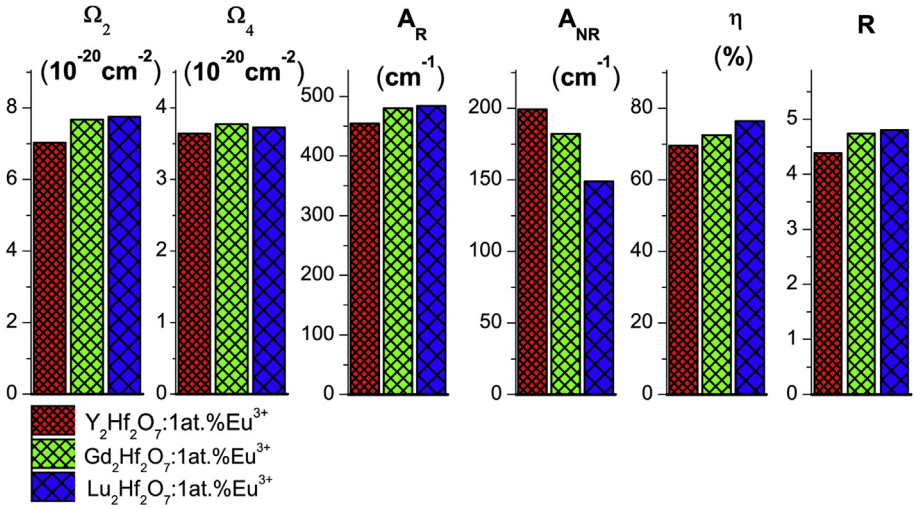

Fig. 6. Judd-Ofelt intensity parameters Ω_2 and Ω_4, experimental lifetimes τ, radiative and non-radiative transition rates A_R and A_{NR}, quantum efficiencies η, and asymmetry ratios R of europium(III) emission from $A_2Hf_2O_7$ (A = Y, Gd, Lu) hosts prepared at 800 °C with 1 at.% europium.

emission follow $Lu_2Hf_2O_7 > Gd_2Hf_2O_7 > Y_2Hf_2O_7$ trend.

Acknowledgment

The authors acknowledge the financial support of the Ministry of Education, Science and Technological Development of the Republic of Serbia (Project no 45020). The work of K. Smits was supported by Latvian National Research Programme IMIS2 (Grant No. 302/2012).

Appendix A. Supplementary data

Supplementary data related to this article can be found at http://dx.doi.org/10.1016/j.optmat.2016.04.007.

References

[1] P. Holtappels, F.W. Poulsen, M. Mogensen, Electrical conductivities and chemical stabilities of mixed conducting pyrochlores for SOFC applications, Solid State Ionics 135 (2000) 675–679.
[2] J.K. Yamamoto, A.S. Bhalla, Microwave dielectric properties of layered perovskite $A_2B_2O_7$ single-crystal fibers, Mater. Lett. 10 (1991) 11–12.
[3] J.B. Goodenough, N. Castellano, Defect pyrochlores as catalyst supports, J. Solid State Chem. 44 (1982) 108–112.
[4] J. Lian, W.J. Weber, W. Jiang, L.M. Wang, L.A. Boatner, R.C. Ewing, Radiation-induced effects in pyrochlores and nanoscale materials engineering, Nucl. Instrum. Methods Phys. Res. Sect. B 250 (2006) 128–136.
[5] M. Mohapatra, B. Rajeswari, N.S. Hon, R.M. Kadam, V. Natarajan, Photoluminescence properties of 'red' emitting $La_2Zr_2O_7$: Eu pyrochlore ceramics for potential phosphor application, J. Lumin. 166 (2015) 1–7.
[6] M.A. Subramanian, G. Aravamudan, G.V. Subba Rao, Oxide pyrochlores – a review, Prog. Solid State Chem. 15 (1985) 55–143.
[7] B.D. Begg, N.J. Hess, D.E. McCready, S. Thevuthasan, W.J. Weber, Heavy-ion irradiation effects in $Gd_2(Ti_{2-x}Zr_x)O_7$ pyrochlores, J. Nucl. Mater. 289 (2001) 188–193.
[8] B.D. McNicol, G.T. Pott, Luminescence of Mn ions in ordered and disordered $LiAl_5O_8$, J. Lumin. 6 (1973) 320–334.
[9] M.G. Brik, A.M. Srivastava, N.M. Avram, Comparative analysis of crystal field effects and optical spectroscopy of six-coordinated Mn^{4+} ion in the $Y_2Ti_2O_7$ and $Y_2Sn_2O_7$ pyrochlores, Opt. Mater. 33 (2011) 1671–1676.
[10] S. Ćulubrk, Ž. Antić, M. Marinović-Cincović, P.S. Ahrenkiel, M.D. Dramićanin, Synthesis and luminescent properties of rare earth (Sm^{3+} and Eu^{3+}) doped $Gd_2Ti_2O_7$ pyrochlore nanopowders, Opt. Mater. 37 (2014) 598–606.
[11] S. Ćulubrk, Ž. Antić, V. Lojpur, M. Marinović-Cincović, M.D. Dramićanin, Sol-gel derived Eu^{3+}-doped $Gd_2Ti_2O_7$ pyrochlore nanopowders, J. Nanomater. 2015 (2015). Article ID 514173.
[12] A. Liqiong, I. Akihiko, G. Takashi, Fabrication of transparent $Lu_2Hf_2O_7$ by reactive spark plasma sintering, Opt. Mater. 35 (2013) 817–819.
[13] B.Z. Zhou, G.H. Zhou, L.Q. An, F. Zhang, G.J. Zhang, S.W. Wang, Morphology-controlled synthesis of yttrium hafnate by oxalate co-precipitation method and the growth mechanism, J. Alloys Compd. 481 (2009) 434–437.
[14] S. Ćulubrk, V. Lojpur, S.P. Ahrenkiel, J.M. Nedeljković, M.D. Dramićanin, Non-contact thermometry with Dy^{3+} doped $Gd_2Ti_2O_7$ nano-powders, J. Lumin. 170 (2016) 395–400.
[15] V. Lojpur, S. Ćulubrk, M.D. Dramićanin, Ratiometric luminescence thermometry with different combinations of emissions from Eu^{3+} doped $Gd_2Ti_2O_7$ nanoparticles, J. Lumin. 170 (2016) 467–471.
[16] R.D. Shannon, Revised effective ionic radii and systematic studies of interatomic distances in halides and chaleogenides, Acta Crystallogr. Sect. A Found. Crystallogr. 32 (1976) 751–767.
[17] C. Karthik, T.J. Anderson, D. Gout, R. Ubic, Transmission electron microscopic study of pyrochlore to defect-fluorite transition in rare-earth pyrohafnates, J. Solid State Chem. 194 (2012) 168–172.
[18] C. Nästren, R. Jardin, J. Somers, M. Walter, B. Brendebach, Actinide incorporation in a zirconia based pyrochlore $(Nd_{1.8}An_{0.2})Zr_2O_{7+x}$ (An= Th, U, Np, Pu, Am), J. Solid State Chem. 182 (2009) 1–7.
[19] G. Zhou, Z. Wang, B. Zhou, Y. Zhao, G. Zhang, S. Wang, Fabrication of transparent $Y_2Hf_2O_7$ ceramics via vacuum sintering, Opt. Mater. 35 (2013) 774–777.
[20] V.G. Sevastyanov, E.P. Simonenko, N.P. Simonenko, V.L. Stolyarova, S.I. Lopatin, N.T. Kuznetsov, Synthesis, vaporization and thermodynamic properties of superfine $Nd_2Hf_2O_7$ and $Gd_2Hf_2O_7$, Eur. J. Inorg. Chem. 26 (2013) 4636–4644.
[21] K. Liao, D.Y. Jiang, Y.M. Ji, J.L. Shi, Combustion synthesis of nanosized $Y_2Hf_2O_7$ and $Lu_2Hf_2O_7$ powders, Key Eng. Mater. 280–283 (2007) 643–646.
[22] K.R. Whittle, L.M.D. Cranswick, S.A.T. Redfern, I.P. Swainson, G.R. Lumpkin, Lanthanum pyrochlores and the effect of yttrium addition in the systems $La_{2-x}Y_xZr_2O_7$ and $La_{2-x}Y_xHf_2O_7$, J. Solid State Chem. 182 (2009) 442–450.
[23] L. Kong, Z. Zhang, M. Reyes, I. Karatchevtseva, G.R. Lumpkin, G. Triani, R.D. Aughterson, Soft chemical synthesis and structural characterization of $Y_2Hf_xTi_{2-x}O_7$, Ceram. Int. 41 (2015) 5309–5317.
[24] Y.K. Liao, D.Y. Jiang, Y.P. Xu, J.L. Shi, Synthesis of ultrafine $Lu_2Hf_2O_7$/Tb phosphor by solution combustion process, Key Eng. Mater 336–338 (2007) 640–642.
[25] R. Giri, Fluorescence quenching of coumarins byhalide ions, Spectrochim. Acta Part A 60 (2004) 757–763.
[26] A.S. Souza, Y.A.R. Oliveira, M.A. Couto dos Santos, Enhanced approach to the Eu^{3+} ion $^5D_0 \rightarrow {}^7F_0$ transition intensity, Opt. Mater. 35 (2013) 1633–1635.
[27] K. Binnemans, Interpretation of europium(III) spectra, Coord. Chem. Rev. 295 (2015) 1–45.
[28] C.A. Kodaira, H.F. Brito, O.L. Malta, O.A. Serra, Luminescence and energy transfer of the europium (III) tungstate obtained via the Pechini method, J. Lumin. 101 (2003) 11–21.
[29] S. Das, A.A. Reddy, S. Ahmad, R. Nagarajan, G.V. Prakash, Synthesis and optical characterization of strong red light emitting $KLaF_4$:Eu^{3+} nanophosphors, Chem. Phys. Lett. 508 (2011) 117–120.
[30] H. Wen, G. Jia, C.K. Duan, P.A. Tanner, Understanding Eu^{3+} emission spectra in glass, Phys. Chem. Chem. Phys. 12 (2010) 9933–9937.
[31] A.K. Vishwakarma, K. Jha, M. Jayasimhadri, A.S. Rao, K. Jang, B. Sivaiah, D. Haranath, Red light emitting $BaNb_2O_6$:Eu^{3+} phosphor for solid state lighting applications, J. Alloys Compd. 622 (2015) 97–101.
[32] M.J. Weber, T.E. Varitimos, B.H. Matsinger, Optical intensities of rare-earth ions in yttrium orthoaluminate, Phys. Rev. B Condens. Matter 8 (1973) 47–53.
[33] J.E. Lowther, Spectroscopic transition probabilities of rare earth ions, J. Phys. C. Solid State Phys. 7 (1974) 4393–4402.

Please cite this article in press as: J. Papan, et al., Europium(III)-doped $A_2Hf_2O_7$ (A = Y, Gd, Lu) nanoparticles: Influence of annealing temperature, europium(III) concentration and host cation on the luminescent properties, Optical Materials (2016), http://dx.doi.org/10.1016/j.optmat.2016.04.007

[34] C. Görller-Walrand, L. Fluyt, A. Ceulemans, W.T. Carnall, Magnetic dipole transitions as standards for Judd-Ofelt parametrization in lanthanide spectra, J. Chem. Phys. 95 (1991) 3099–3106.
[35] B.R. Judd, Optical absorption intensities of rare-earth ions, Phys. Rev. 127 (1962) 750–761.
[36] G.S. Ofelt, Intensities of crystal spectra of rare-earth ions, J. Chem. Phys. 37 (1962) 511–520.
[37] M.H.V. Werts, R.T.F. Jukes, J.W. Verhoeven, The emission spectrum and the radiative lifetime of Eu^{3+} in luminescent lanthanide complexes, Phys. Chem. Chem. Phys. 4 (2002) 1542.
[38] Lj. Djačanin, S.R. Lukić, D.M. Petrović, M. Nikolić, M.D. Dramićanin, Judd-Ofelt analysis of luminescence emission from Zn_2SiO_4:Eu^{3+} nanoparticles obtained by a polymer-assisted sol gel method, Phys. B Condens. Matter 406 (2011) 2319–2322.
[39] W.T. Carnall, P.R. Fields, K. Rajnak, Electronic energy levels in the trivalent lanthanide aquo ions. I. Pr3+, Nd3+, Pm3+, Sm3+, Dy3+, Ho3+, Er3+, and Tm3+, J. Chem. Phys. 49 (1968) 4424.
[40] M.J. Weber, Handbook of Optical Materials, CRC Press, Boca Raton, FL, 2003.
[41] K. Binnemans, K. Van Herck, C. Görller-Walrand, Influence of dipicolinate ligands on the spectroscopic properties of europium(III) in solution, Chem. Phys. Lett. 266 (1997) 297–302.
[42] M. Kumar, T.K. Seshagiri, S.V. Godbole, Fluorescence lifetime and judd–Ofelt parameters of Eu3+ doped SrBPO5, Phys. Rev. B Condens. Matter 410 (2013) 141–146.
[43] R. Reisfeld, E. Zigansky, M. Gaft, Europium probe for estimation of site symmetry in glass films, glasses and crystals, Mol. Phys. 102 (2004) 1319–1330.
[44] K. Gatterer, G. Pucker, H.P. Fritzer, Structural information in the optical spectra of Eu^{3+} doped glasses from the ternary system Na_2O-B_2O_3-SiO_2, Phys. Chem. Glas. 38 (1997) 293–299.
[45] Y.C. Li, Y.H. Chang, Y.F. Lin, Y.S. Chang, Y.J. Lin, Synthesis and luminescent properties of Ln^{3+} (Eu^{3+}, Sm^{3+}, Dy^{3+})-doped lanthanum aluminum germanate $LaAlGe_2O_7$ phosphors, J. Alloys Compds. 439 (2007) 367–375.
[46] G. Blasse, G. Dirksen, A simple luminescence experiment suggesting rare earth ion pairing in the fluorite structure, J. Electrochem. Soc. 127 (4) (1980) 978–979.
[47] K. Smits, L. Grigorjeva, D. Millers, A. Sarakovskis, A. Opalinska, J.D. Fidelus, W. Lojkowski, Europium doped zirconia luminescence, Opt. Mater. 32 (8) (2010) 827–831.

Please cite this article in press as: J. Papan, et al., Europium(III)-doped $A_2Hf_2O_7$ (A = Y, Gd, Lu) nanoparticles: Influence of annealing temperature, europium(III) concentration and host cation on the luminescent properties, Optical Materials (2016), http://dx.doi.org/10.1016/j.optmat.2016.04.007